

Motion of a helical vortex

Oscar Velasco Fuentes

Departamento de Oceanografía Física, CICESE, Ensenada, México

Email address: ovelasco@cicese.mx

Submitted to the European Journal of Mechanics B/fluids, 30 July 2015

Abstract

We study the motion of a single helical vortex in an unbounded, inviscid, incompressible fluid. The vortex is an infinite tube whose centerline is a helix and whose cross section is a circle of small radius (compared to the radius of curvature) where the vorticity is uniform and parallel to the centerline. Ever since Joukowski (1912) deduced that this vortex translates and rotates steadily without change of form, numerous attempts have been made to compute these self-induced velocities. Here we use Hardin's (1982) solution for the velocity field to find new expressions for the vortex's linear and angular velocities. Our results, verified by numerically computing the Helmholtz integral and the Rosenhead-Moore approximation to the Biot-Savart law, are more accurate than previous results over the whole range of values of the vortex pitch and cross-section. We then use the new formulas to study the advection of passive particles near the vortex; we find that the vortex's motion and capacity to transport fluid depend on its pitch and cross section as follows: a thin vortex of small pitch moves fast and carries a small amount of fluid; a thick vortex of small pitch moves at intermediate velocities and is a moderate carrier itself but it pushes fluid forward along the helix axis; and a vortex of large pitch, whether thin or thick, moves slowly and carries a large amount of fluid.

1 Introduction

The realisation that concentrated helical vortices are frequent features in natural and man-made flows has grown steadily since Parsons (1901) discovered that “a small spiral vortex existed just behind the tips of the propeller blades” used to generate thrust to propel a vessel. The theoretical study

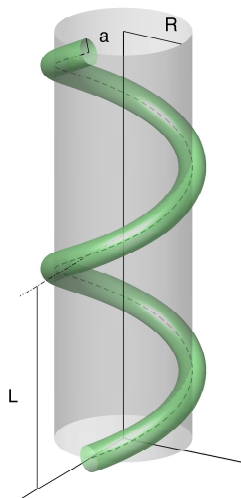


Figure 1: A segment of a thin helical vortex. The vortex extends indefinitely in both directions and its centerline is a helix of pitch L and radius R lying on the surface of an imaginary supporting cylinder.

of helical vortices has an even longer history. Here we highlight the earliest results, but see Ricca (1994) for a detailed review of classical studies of the self-induced velocity of a single helical vortex in an inviscid, unbounded fluid (figure 1). Kelvin (1880) found that one mode of vibration of a cylindrical vortex is a wave that deforms the vortex axis into a helix of small radius and large pitch, and that this wave propagates along the axis with constant speed. Fitzgerald (1899) assumed that this result was valid for helices of any pitch and radius and speculated about the flow induced by the vortex: “there will be, on the whole, a flow along the inside of the spiral, but the motion of the fluid is complex.” Joukowski (1912) showed that a helical vortex moves steadily without change of form and found that its self-induced velocity is approximately equal to the velocity of an osculating ring vortex; he further stated that any number of equal helical vortices symmetrically arranged with respect to a common axis form a steadily moving arrangement.

In the last two decades there has been a renewed interest on helical vortices (Ricca, 1994; Mezić et al., 1998; Kuibin and Okulov, 1998; Boersma and Wood, 1999; Wood and Boersma, 2001; Okulov, 2004). Some of these works have concentrated on the binormal component of the self-induced

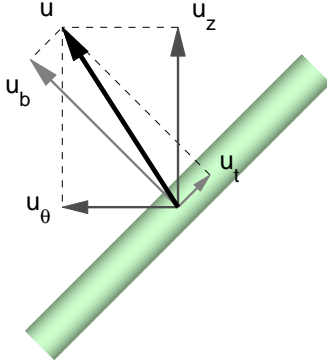


Figure 2: The self-induced velocity of a helical vortex, u , represented as the sum of either the azimuthal and axial components (u_θ and u_z , respectively) or the tangential and binormal components (u_t and u_b , respectively).

velocity and have implicitly or explicitly dismissed the tangential component (see figure 2). This is unfortunate because accurate values of the full self-induced velocity are essential for a proper analysis of the vortex stability (see, e.g., Widnall, 1972) or the particle motion in the vicinity of the vortex (see, e.g., Mezić et al., 1998; Andersen and Brøns, 2014).

The objectives of this paper are, first, to obtain expressions for the vortex's linear and angular velocities (U and Ω , respectively) that are accurate over the whole range of pitch values for vortices of small cross section (when compared to the radius of curvature of their centerline); and, second, to apply the new formulas in the study of particle motion in the flow induced by helical vortices. Section 2 contains our theoretical calculations, which are based on the velocity field obtained by Hardin (1982); the verification of the new formulas for U and Ω by numerical computation of the Helmholtz integral and the Rosenhead-Moore approximation to the Biot-Savart law; and a comparison with previous results (Joukowsky, 1912; Da Rios, 1916; Levy and Forsdyke, 1928; Widnall, 1972; Mezić et al., 1998; Okulov, 2004). In section 3 we determine the vortex's capacity to carry fluid by analysing the helical stream function of Hardin (1982) in a system that moves with the vortex. We present our conclusions in section 4.

2 Self-induced motion of the vortex

A helical vortex is a thin tube of infinite length whose centerline is a helix of uniform pitch lying on the surface of an imaginary supporting cylinder (see figure 1). The centerline of the vortex is given, in Cartesian coordinates, as follows:

$$\begin{aligned}x &= R \cos \theta, \\y &= R \sin \theta, \\z &= L\theta/2\pi,\end{aligned}$$

where θ is the angle around the cylinder's axis, R is the radius of the helix and L is the pitch of the helix.

On the vortex's circular cross-section the vorticity is uniform in magnitude and direction, which is parallel to the centerline's tangent. Note that both, the circular shape and the uniform vorticity, are leading-order approximations only: in a steady solution of the Euler equations the vorticity varies linearly with the distance to the centre of curvature and the cross-section is a small perturbation of the circular shape. The vortex thus has circulation $\Gamma = \pi a^2 \omega$, where a is the radius of the cross-section and ω is the magnitude of the vorticity. The four parameters that uniquely define the vortex are then Γ , R , L and a but, since the value of Γ merely changes the time scale of the evolution, we are left with two non-dimensional parameters: the vortex radius $\alpha = a/R$ and the vortex pitch $\tau = L/2\pi R$.

2.1 Analytical results

Because of the geometry of the problem the self-induced velocity of the vortex can be expressed in either cylindrical components, u_θ , u_z , pointing in the azimuthal and axial directions, respectively; or in natural components, u_t , u_b , pointing in the tangent and binormal directions, respectively (see figure 2). We will use cylindrical coordinates instead of the now more popular natural coordinates because the translation speed of the vortex, U , equals the axial component of the self-induced velocity, u_z , whereas the angular velocity of the vortex, Ω , equals the azimuthal component divided by the helix radius, u_θ/R .

Hardin (1982) found the velocity field produced by an infinitely-thin helical vortex. His solution, expressed in cylindrical coordinates, is divided in an interior field (valid inside the supporting cylinder) and an exterior field (valid outside the supporting cylinder). Here we reproduce only the

azimuthal and axial components needed for the calculation of the vortex motion:

$$u_\theta(r, \phi) = \begin{cases} \frac{\Gamma R}{\pi r l} S_1(r, \phi) & \text{if } r < R \\ \frac{\Gamma}{2\pi l} + \frac{\Gamma R}{\pi r l} S_2(r, \phi) & \text{if } r > R \end{cases} \quad (1)$$

$$u_z(r, \phi) = \begin{cases} \frac{\Gamma}{2\pi l} - \frac{\Gamma R}{\pi l^2} S_1(r, \phi) & \text{if } r < R \\ -\frac{\Gamma R}{\pi l^2} S_2(r, \phi) & \text{if } r > R \end{cases} \quad (2)$$

where $\phi = \theta - z/l$, $l = L/2\pi$ and

$$S_1(r, \phi) = \sum_{m=1}^{\infty} m K'_m \left(\frac{mR}{l} \right) I_m \left(\frac{mr}{l} \right) \cos m\phi$$

$$S_2(r, \phi) = \sum_{m=1}^{\infty} m K_m \left(\frac{mr}{l} \right) I'_m \left(\frac{mR}{l} \right) \cos m\phi$$

are Kapteyn series involving the modified Bessel functions K_m and I_m , and their corresponding derivatives K'_m and I'_m .

Since we are dealing with vortices of finite cross section, it is possible to compute the vortex's self-induced velocity by evaluating the velocity field at two diametrically-opposed points on the surface of the tubular vortex. The uniformity of the vorticity on the cross section guarantees that the average of these velocities is the actual velocity at the centerline, i.e. the velocity of the vortex. This approach has been previously used by Ricca (1994), Boersma and Wood (1999), and Okulov (2004) for the computation of the binormal component; here we will use it for the computation of the axial and azimuthal components. For simplicity, we choose to evaluate the velocity at points $(r, \theta, z) = (R \pm a, 0, 0)$ or, in helical coordinates, $(r, \phi) = (R \pm a, 0)$. Therefore, the self-induced motion of the vortex is given by

$$U = \frac{1}{2} [u_z(R - a, 0) + u_z(R + a, 0)] \quad (3)$$

$$\Omega = \frac{1}{2R} [u_\theta(R - a, 0) + u_\theta(R + a, 0)] \quad (4)$$

A technical issue with this method is that the series S_1 and S_2 converge slowly, particularly when approaching the vortex itself, which hinders the computation of U and Ω . This problem was solved by Boersma and Wood

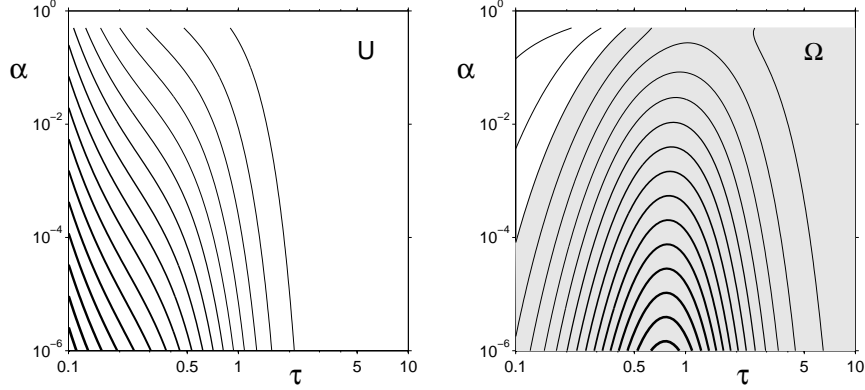


Figure 3: The linear and angular velocities of a helical vortex (U and Ω , respectively) as functions of its pitch and radius (τ and α , respectively). The thick contours indicate higher absolute values of U or Ω ; the grey areas indicate the region of the parameter space where Ω is negative (clockwise rotation of the helix).

(1999), who eliminated the singularities from S_1 and S_2 for the two particular points needed in the computation of the self induced motion:

$$S_1(R - a, 0) = \frac{1}{4} \frac{\tau^2}{(1 + \tau^2)^{3/2}} \left(-\frac{2}{\epsilon} + \ln(\epsilon) + \ln \left(\frac{\sqrt{1 + \tau^2}}{2} \right) \right) + \frac{\tau}{2} - \frac{\tau^2}{4} W(\tau) + o(1)$$

$$S_2(R + a, 0) = \frac{1}{4} \frac{\tau^2}{(1 + \tau^2)^{3/2}} \left(\frac{2}{\epsilon} + \ln(\epsilon) + \ln \left(\frac{\sqrt{1 + \tau^2}}{2} \right) \right) - \frac{\tau^2}{4} W(\tau) + o(1)$$

where $\epsilon = a/R(1 + \tau^2)$, $o(1)$ represents an expression that tends to 0 when $\epsilon \rightarrow 0$, and

$$W(\tau) = \int_0^\infty \left[\frac{\sin^2 t}{(\tau^2 t^2 + \sin^2 t)^{3/2}} - \frac{1}{(1 + \tau^2)^{3/2}} \frac{H(1/2 - t)}{t} \right] dt$$

with $H(\cdot)$ the unit step function. Boersma and Wood (1999) computed $W(\tau)$ by numerical quadrature for 21 values of τ in the range $[0.01 - 10]$ and obtained approximate analytical forms for large values of τ (giving less than 1% error for $\tau \geq 3$) and for small values of τ (giving less than 1% error for $\tau \leq 0.4$). Here we computed the value of $W(\tau)$ using the numerical method described by Boersma and Wood (1999).

The substitution of these forms of S_1 and S_2 in (1)-(2) and the subsequent substitution of the resulting expressions for u_θ and u_z in (3)-(4) give,

after some algebra, the linear and angular velocities in nondimensional form:

$$U^* = \frac{1}{(1 + \tau^2)^{3/2}} \left(\ln(2/\epsilon) - \ln(\sqrt{1 + \tau^2}) + (1 + \tau^2)^{3/2} W(\tau) \right)$$

$$\Omega^* = \frac{\tau}{(1 + \tau^2)^{3/2}} \left(\frac{2(1 + \tau^2) + \ln(2/\epsilon) - \ln(\sqrt{1 + \tau^2}) - (1 + \tau^2)^{3/2}(2/\tau - W(\tau))}{\epsilon^2(1 + \tau^2)^2 - 1} \right)$$

In dimensional form the self-induced motion of the vortex is given by

$$U = \frac{\Gamma}{4\pi R} U^* \quad (5)$$

$$\Omega = \frac{\Gamma}{4\pi R^2} \Omega^* \quad (6)$$

Figure 3 shows U and Ω in the region $10^{-6} < \alpha < 0.4$ and $0.1 < \tau < 10$. All vortices translate in the direction of the axial component of the vorticity with a velocity U that increases as their pitch τ and radius α decrease. The vortices generally rotate in a direction opposite to the azimuthal component of the vorticity, i.e. clockwise when seen from the direction in which the vortex translates. They rotate with an angular velocity Ω that, for a fixed radius α , has a maximum absolute value when their pitch τ is about one and that, for a fixed τ , increases in magnitude as α decreases. Only relatively thick vortices of small pitch rotate in anti-clockwise sense (upper left corner in figure 3).

Note that the translation speed U behaves as the helix's curvature, $1/R(1 + \tau^2)$, which has a maximum value $(1/R)$ when $\tau = 0$ and then decreases to zero as τ goes to infinity. Similarly, the magnitude of the rotation speed Ω behaves as the helix's torsion, $\tau/R(1 + \tau^2)$, which grows from zero when $\tau = 0$ to its maximum value $(1/2R)$ when $\tau = 1$ and then decreases to zero as τ goes to infinity.

2.2 Comparison with numerical results

We verified equations (5) and (6) by computing the self-induced velocities of the vortex by numerical integration of the Helmholtz formula,

$$\mathbf{u}(\mathbf{x}) = -\frac{1}{4\pi} \int \frac{[\mathbf{x} - \mathbf{x}'] \times \boldsymbol{\omega}}{|\mathbf{x} - \mathbf{x}'|^2} dV, \quad (7)$$

and the Rosenhead-Moore approximation to the Biot-Savart law,

$$\mathbf{u}(\mathbf{x}) = -\frac{\Gamma}{4\pi} \int \frac{[\mathbf{x} - \mathbf{r}(s)] \times d\mathbf{s}}{(|\mathbf{x} - \mathbf{r}(s)|^2 + \mu^2 a^2)^{3/2}}, \quad (8)$$

where a is the radius of the cross section of the tubular vortex and μ is a parameter that depends on the vortex local structure, i.e. its vorticity distribution, curvature and torsion. Since, by our definition, a helical vortex has everywhere the same local structure μ is a constant but its value must be determined. This is usually done by choosing μ so that the integral (8) produces results in agreement with a known solution obtained with a different method (see, e.g., Saffman, 1995). Here we use $\mu = e^{-3/4}$ because this value leads to the correct velocity for a ring vortex of uniform vorticity, constant curvature and zero torsion; this choice may thus be expected to give a good approximation for a helical vortex of uniform vorticity, constant curvature and constant torsion.

In the computation of the Rosenhead-Moore integral we used a single filament represented by M nodes. In the computation of the Helmholtz integral we used 100 filaments, each represented by M nodes; none of these filaments coincides with the vortex centerline so, in contrast to the Biot-Savart case, there is no need to smooth out the singularity and, consequently, there is no free tuning parameter in (7). The value of M varied between 10^3 and 10^4 depending on the helix pitch L .

In order to compare the numerical and analytical results, we define the relative difference between them as follows

$$D_T = \left(\frac{(U_n - U)^2 + (R\Omega_n - R\Omega)^2}{U^2 + (R\Omega)^2} \right)^{1/2}$$

where quantities without subscript are obtained with formulas (5)-(6) and those with subscript are obtained with either equation (7) or (8). We also find useful to define the relative difference between the linear velocities, $D_U = |U_n - U|/U$, and the absolute difference between the angular velocities, $\Delta\Omega = |\Omega_n - \Omega|$ (we must use this because Ω is zero on a curve $\alpha = f(\tau)$, see figure 3, and the relative difference would grow indefinitely even if the absolute difference were within round-off error).

Figure 4 shows D_U , D_Ω and D_T as functions of the vortex pitch ($0.1 < \tau < 10$) for a given vortex radius ($\alpha = 0.05$). In this case the velocities computed with (5)-(6) and the Helmholtz integral have a mean relative difference $D_T = 0.17\%$ with a maximum of 0.27% at $\tau \approx 0.65$. In contrast, when the former are compared with Rosenhead-Moore calculations (using $\mu = e^{-3/4}$) the mean relative difference is 4.6% with a maximum of 5.7% at $\tau \approx 1.4$, the maximum D_U is 4.7% at $\tau \approx 1$, and the maximum $\Delta\Omega$ occurs at $\tau \approx 0.7$. It is significant that the largest differences are obtained for vortices with high torsion, for it must be remembered that $\mu = e^{-3/4}$ is tuned to produce the correct velocity of a vortex of zero torsion. Therefore we varied

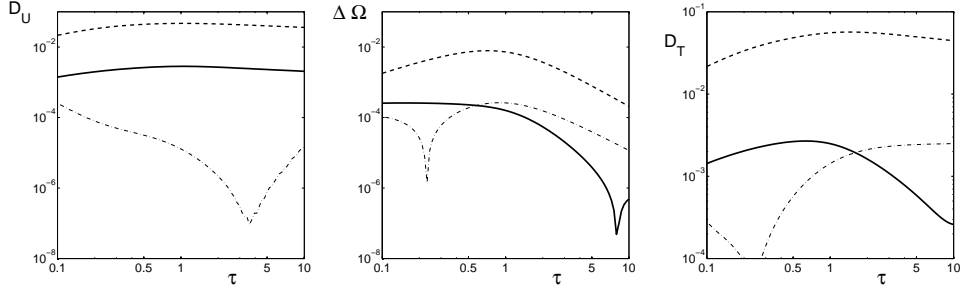


Figure 4: The relative difference in linear velocity D_U , the absolute difference in angular velocity $\Delta\Omega$, and the relative difference in total velocity D_T , as functions of the vortex pitch (τ), for a given vortex radius ($\alpha = 0.05$). Results obtained with equations 5-6 are compared with numerical integration of equation 7 (continuous line), equation 8 using $\mu = e^{-3/4}$ (dashed line), and equation 8 using $\mu = e^{-1}$ (dash-dotted line).

the parameter μ in order to achieve a better agreement and found that $\mu = e^{-1}$ produces a mean relative difference $D_T = 0.13\%$ with a maximum of 0.25% .

Identical results in D_U , D_Ω and D_T are obtained if the Rosenhead-Moore kernel is replaced by the Winckelmans-Leonard kernel (Winckelmans and Leonard, 1993); i.e., if instead of equation (8) we use

$$\mathbf{u}(\mathbf{x}) = -\frac{\Gamma}{4\pi} \int \frac{|\mathbf{x} - \mathbf{r}(s)|^2 + \frac{5}{2}\mu^2 a^2}{(|\mathbf{x} - \mathbf{r}(s)|^2 + \mu^2 a^2)^{5/2}} [\mathbf{x} - \mathbf{r}(s)] \times d\mathbf{s}.$$

With this kernel it is $\mu = e^{-1/4}$ which leads to the correct ring-vortex velocity and 6% differences between analytically and numerically computed velocities of helical vortices, whereas $\mu = e^{-1/2}$ brings these differences down to 0.25% .

2.3 Comparison with previous results

Joukowski (1912) and Da Rios (1916) found that, to the order of approximation they used, the self-induced velocity is entirely in the binormal direction.

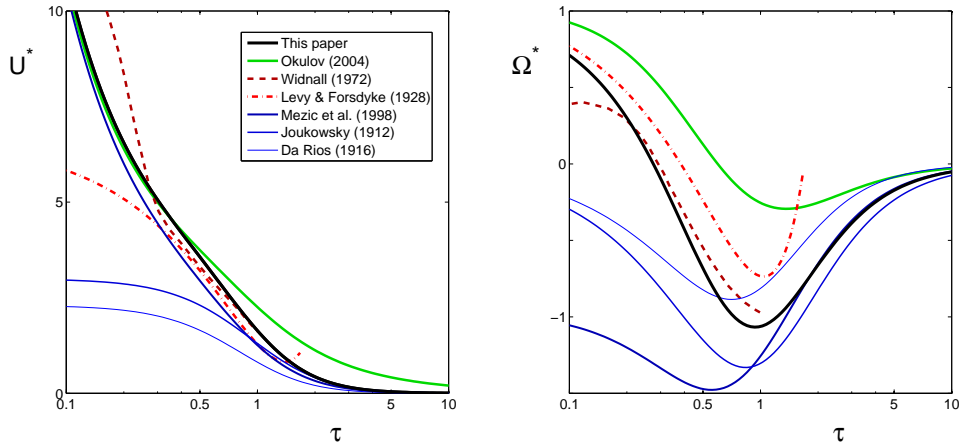


Figure 5: Linear and angular velocities, U and Ω , respectively, as functions of the vortex pitch (τ), for a given vortex radius ($\alpha = 0.1$).

They found the binormal velocity, u_b , to be given by

$$u_b = \begin{cases} \frac{\Gamma}{4\pi R_c} \log\left(\frac{2R_c}{a}\right) & \text{(Joukowsky 1912)} \\ \frac{\Gamma}{4\pi R_c} \log\left(\frac{1}{a}\right) & \text{(Da Rios, 1916)} \end{cases} \quad (9)$$

where $R_c = R(1 + \tau^2)$ is the radius of curvature. Note that the formula of Da Rios (1916) is a straightforward application of the localised induction approximation he introduced ten years earlier (Da Rios, 1906). We decomposed these velocities in cylindrical components in order to compute U and Ω (see the thin blue lines in figure 5); they are in reasonably good agreement with (5)–(6), shown in black thick lines, for $\tau > 2$ only.

Levy and Forsdyke (1928) and Widnall (1972) computed the linear velocity U and the angular velocity Ω of helical vortices of small pitch (in the ranges $0.25 < \tau < 1.25$ and $0.1 < \tau < 1$, respectively). Levy and Forsdyke (1928) avoided the singularity in the Biot-Savart law by evaluating part of the integral near, instead of on, the filament; Widnall (1972) obtained the self-induced velocity using the cut-off method and matched asymptotic expansions. In the range $0.3 < \tau < 1$ the results of Widnall (1972) and Levy and Forsdyke (1928), shown in dashed and dash-dotted lines in figure 5, are in better agreement with equations (5)–(6) than any earlier or later result.

Ricca (1994), Boersma and Wood (1999) and Mezić et al. (1998) argued

that the tangential component is unimportant and computed the binormal component only. It is true that the former contributes nothing to the time evolution of the Eulerian velocity field but it cannot be neglected in the analysis of particle motion (in section 3 we will show that neglecting the tangential component, which can reach up to 30 % of the value of the binormal component for relatively thick vortices of small pitch, leads to significant errors in the determination of the flow topology and the capacity of the vortex to carry fluid). Mezić et al. (1998) decomposed the binormal velocity u_b to obtain U and Ω : the former shows reasonable agreement with (5) for all values of the vortex pitch, the latter shows good agreement with (6) for $\tau > 1$ only.

The results of Okulov (2004) for the binormal component (u_b , not shown here) are in good agreement with ours; his results for U and Ω , shown in green lines in figure 5, differ greatly from ours as a consequence of his use of inconsistent assumptions, as explained below. In what follows the prefixes “O” and “R” indicate equations in Okulov (2004) and Ricca (1994), respectively. Equation O4.4, which gives Ω as a function of τ and u_b , was obtained using O2.4 and transformation relations between cylindrical and natural components (see R4.1). Then u_b was computed under the assumption that the vorticity is uniform on the vortex cross section (see O4.6 and R4.12). A conflict exists because O2.4 implies O2.9, which means that the vorticity is parallel to helical lines of constant dimensional pitch ($l = L/2\pi$). Such a vorticity field cannot be uniform on the vortex cross section; thus O4.4 gives an incorrect value of Ω . The same conflicting assumptions are used by Okulov and Sørensen (2007, 2010).

3 Flow topology

With an appropriate change of variables it is possible to write the velocity field (u_r, u_θ, u_z) in terms of a stream function (Hardin, 1982). If we define $\phi = \theta - z/l$ then $u_\phi = u_\theta - ru_z/l$ and the velocity field is given by

$$\begin{aligned} u_r &= \frac{1}{r} \frac{\partial \psi}{\partial \phi} \\ u_\phi &= -\frac{\partial \psi}{\partial r} \end{aligned}$$

with the stream function defined as follows (Hardin, 1982):

$$\psi(r, \phi) = \begin{cases} \frac{\Gamma(r^2 - R^2)}{4\pi l^2} - \frac{\Gamma R r}{\pi l^2} S_3(r, \phi) & \text{if } r < R \\ \frac{\Gamma}{2\pi} \log\left(\frac{R}{r}\right) - \frac{\Gamma R r}{\pi l^2} S_4(r, \phi) & \text{if } r > R \end{cases}$$

where

$$S_3(r, \phi) = \sum_{m=1}^{\infty} K'_m \left(\frac{mR}{l}\right) I'_m \left(\frac{mr}{l}\right) \cos m\phi$$

$$S_4(r, \phi) = \sum_{m=1}^{\infty} K'_m \left(\frac{mr}{l}\right) I'_m \left(\frac{mR}{l}\right) \cos m\phi$$

The stream function gives information about particle motion only if the flow is stationary. The flow induced by a helical vortex is time dependent in a reference frame fixed in space, but it can be made time independent in an infinite number of moving frames. The most natural choice, and the only one giving information about the capacity of the vortex to carry fluid, is a reference frame where the vortex is stationary; that is to say, in a frame that translates with linear velocity U and rotates with angular velocity Ω . The steady stream function Ψ is obtained with the simple transformation

$$\Psi = \psi + \frac{1}{2} \left(\Omega - \frac{U}{l} \right) r^2 \quad (10)$$

Because of the definition $\phi = \theta - z/l$, the curves of constant Ψ , which are streamlines of the helical flow (u_r, u_ϕ) , represent the intersections of the stream surfaces of the three-dimensional flow (u_r, u_θ, u_z) with the polar plane $z = 0$. The intersections of the same stream surfaces with the meridional planes $\theta = 0, \pi$ can be readily obtained using the same definition.

The flow topology, or phase portrait in the language of dynamical-systems, consist of the set of stagnation points plus the streamlines that divide the flow in regions of qualitatively different behaviour. In the co-moving frame the vortex, located at $(r, \theta) = (a, 0)$, corresponds to a stagnation point of elliptic type and the symmetries of Ψ indicate that other fixed points, when they exist, are located on the line $\theta = 0, \pi$. We found these stagnation points using a numerical method in order to perform a systematic exploration of the region of the parameter space defined by $10^{-6} < \alpha < 0.4$ and $0.1 < \tau < 10$.

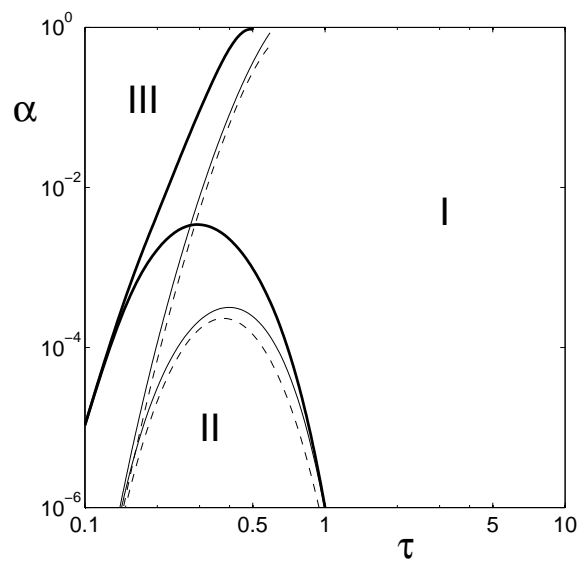


Figure 6: The three flow regimes in the parameter plane (τ, α) : (I) large-pitch helices; (II) thin small-pitch helices; and (III) thick small-pitch helices. The thick lines show the boundaries found in this work, the thin lines show those found by Mezić et al. (1998) and the dashed lines show the results of Andersen and Brøns (2014).

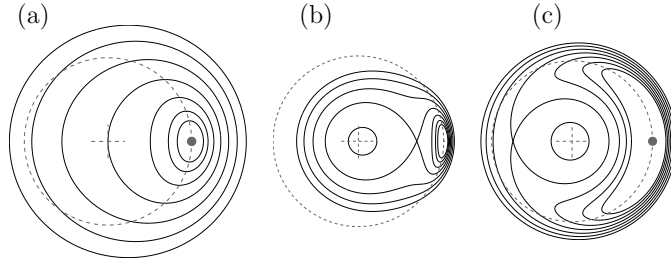


Figure 7: The helical stream function Ψ on the polar plane (r, θ) for representative cases of each regime: (a) Large-pitch helices ($\tau=0.8$, $\alpha=0.05$), (b) thin small-pitch helices ($\tau=0.3$, $\alpha=0.0001$), and (c) thick small-pitch helices ($\tau=0.2$, $\alpha=0.05$).

We found three qualitatively different flow topologies (figure 6). These were first identified by Mezić et al. (1998) and Andersen and Brøns (2014); they, however, only took into account the binormal component of the vortex motion: Mezić et al. (1998) computed u_b using the results of Ricca (1994) whereas Andersen and Brøns (2014) used equation (9) with $\log(R_c/a)$. As shown by the blue lines in figure 5 all calculations that do not include the tangential component give large errors in U and Ω , particularly for small values of the vortex pitch ($\tau < 1$). Consequently Mezić et al. (1998) and Andersen and Brøns (2014) found regime boundaries that are significantly shifted from the ones found here (see the thin lines in figure 6).

The properties of each flow topology, and the consequences for the vortex's capacity to carry fluid, are the following:

Regime I (which occupies mostly $\tau > 1$ for all values of α , see figure 6) is characterised by the existence of only one stagnation point in the plane $r-\theta$, this is of elliptic type and coincides with the vortex itself (see figure 7a). The presence of only one elliptic stagnation point implies that all particles have, qualitatively, the same behaviour: they all rotate around the vortex. There is, however, an important quantitative difference: while the particles that are close to the vortex drift slowly downwards, the particles that are farther from it drift with a speed that rapidly approaches $-U$ (figure 8a). In the fixed frame this means that nearby particles follow the vortex in its translation while distant particles remain close to the horizontal plane where they were initially located.

Regime II (which occupies roughly $\tau < 1$ and $\alpha < 0.003$, see figure 6) is characterised by the existence of two elliptic stagnation points and a hyperbolic stagnation point between them (see figure 7b). Now there are three

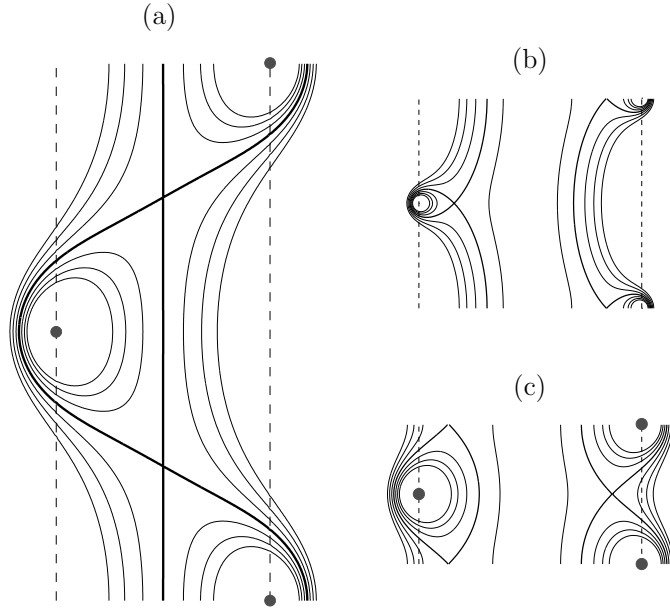


Figure 8: Same as figure 7 but now on the meridional planes (r, z) corresponding to $\theta = 0, \pi$.

regions with qualitatively different behaviour: one set of particles rotate around the vortex and are permanently trapped by it; a second set of particles rotate around a line close to the helix axis while drifting downwards; and the exterior particles rotate around those two sets while drifting downwards (see figure 8b).

Regime III (which occupies roughly $\tau < 0.4$ and $\alpha > 0.0001$, see figure 6) is characterised by the existence of two elliptic stagnation points and a hyperbolic stagnation point next to them (see figure 7c). There are again three regions with qualitatively different behaviour: one set of particles rotate anti-clockwise around the vortex and are permanently trapped by it; a second set of particles rotate clockwise around a line close to the helix axis while drifting upwards; and the exterior particles rotate anti-clockwise around those two sets while drifting downwards (see figure 8c). This is the type of flow Fitzgerald (1899) speculated about.

4 Conclusions

We have found new expressions for the linear and angular velocities of helical vortices that have, to leading order, uniform vorticity and circular cross-section. These expressions are valid for vortices of any pitch (τ) when their cross-sectional radius (α) is much smaller than their radius of curvature (i.e., $\alpha \ll 1 + \tau^2$).

Numerical computations of the motion of helical vortices using the Helmholtz integral and the Rosenhead-Moore approximation to the Biot-Savart law show that the new formulas give the correct velocities or, at least, very good approximations. Indeed, if we assume that $\mu = e^{-3/4}$ in the Rosenhead-Moore kernel leads to the correct velocity then the best approximations are given by the new formulas, within 6 %; Widnall (1972), 13.6 %; and Levy and Forsdyke (1928), 13.9 %. If, on the other hand, we assume that it is $\mu = e^{-1}$ that leads to the correct velocity then the best approximations are given by the new formulas, within 0.5 %; Widnall (1972), 14.1 %; and Mezić et al. (1998), 17.8 %. In any case, equations (5)-(6) give the best approximation published so far.

The pitch and radius of the vortex determine its motion and capacity to carry fluid in the following manner: large-pitch vortices, whether thin or thick, translate slowly and carry with them a large volume of fluid; thin small-pitch vortices translate fast and take with them a small volume of fluid; and thick small-pitch vortices translate at intermediate velocities, take with them a moderate volume of fluid and, more importantly, push fluid forward along the helix axis.

Acknowledgments

This research was partially supported by CONACyT (México) under grant number 169574.

References

- M. Andersen and M. Brøns. Topology of helical fluid flow. *European J. Appl. Mech.*, 25:275–396, 2014.
- J. Boersma and D.H. Wood. On the self-induced motion of a helical vortex. *J. Fluid Mech.*, 384:263–280, 1999.

- L.S. Da Rios. Sul moto d'un liquido indefinito con un filetto vorticoso di forma qualunque. *Rendiconti del Circolo Matematico di Palermo*, 22:117–137, 1906.
- L.S. Da Rios. Vortici ad elica. *Il Nuovo Cimento*, 11:419–431, 1916.
- G.F. Fitzgerald. On a hydro-dynamical hypothesis as to electro-magnetic actions. *The Scientific Proceedings of the Dublin Royal Society*, 9:55–59, 1899.
- J.C. Hardin. The velocity field induced by a helical vortex filament. *Physics of Fluids*, 25:1949–1952, 1982.
- N.E. Joukowski. Vihrevaja teorija grebnoga vinta. *Trudy Otdeleniya Fizicheskikh Nauk Obshchestva Lubitelei Estestvoznaniya*, 16:1–31, 1912. French translation in *Théorie tourbillonnaire de l'hélice propulsive* (Gauthier-Villars, Paris, 1929) 1–47.
- P.A. Kuibin and V. L. Okulov. Self-induced motion and asymptotic expansion of the velocity field in the vicinity of a helical vortex filament. *Physics of Fluids*, 10:607–614, 1998.
- H. Levy and A. G. Forsdyke. The steady motion and stability of a helical vortex. *Proceedings of the Royal Society of London A*, 120:670–690, 1928.
- I. Mezić, A. Leonard, and S. Wiggins. Regular and chaotic particle motion near a helical vortex filament. *Physica D*, 111:179–201, 1998.
- V. L. Okulov. On the stability of multiple helical vortices. *J. Fluid Mech.*, 521:319–342, 2004.
- V. L. Okulov and J.N. Sørensen. Stability of helical tip vortices in a rotor far wake. *J. Fluid Mech.*, 576:1–25, 2007.
- V. L. Okulov and J.N. Sørensen. Maximum efficiency of wind turbine rotors using joukowski and betz approaches. *J. Fluid Mech.*, 649:497–508, 2010.
- C.A. Parsons. The marine steam turbine and its application to fast vessels. *Transactions of the Institution of Engineers and Shipbuilders in Scotland*, 44:175–221, 1901.
- R.L. Ricca. The effect of torsion on the motion of a helical vortex filament. *J. Fluid Mech.*, 273:241–259, 1994.
- P. G. Saffman. *Vortex Dynamics*. Cambridge University Press, 1995.

- W. Thomson (Lord Kelvin). Vibrations of a columnar vortex. *Proceedings of the Royal Society of Edinburgh*, 10:443–456, 1880.
- S.E. Widnall. The stability of a helical vortex filament. *J. Fluid Mech.*, 54: 641–663, 1972.
- G.S. Winckelmans and A. Leonard. Contributions to vortex particle methods for the computation of three-dimensional incompressible unsteady flows. *J. Comp. Phys.*, 109:247–273, 1993.
- D.H. Wood and J. Boersma. On the motion of multiple helical vortices. *J. Fluid Mech.*, 447:149–171, 2001.